






High-temperature superconductivity in electrides dominated by hybridized *p*-orbital-like electride states

Zhao Liu ¹, Defang Duan ², Quan Zhuang ^{3,*}, and Tian Cui ^{1,2,†}

¹*Institute of High Pressure Physics, School of Physical Science and Technology, Ningbo University, Ningbo 315211, People's Republic of China*

²*State Key Laboratory of Superhard Materials, College of Physics, Jilin University, Changchun 130012, People's Republic of China*

³*Inner Mongolia Key Laboratory of Carbon Nanomaterials, Nano Innovation Institute (NII), College of Chemistry and Materials Science, Inner Mongolia Minzu University, Tongliao 028000, People's Republic of China*

 (Received 29 March 2022; revised 23 July 2023; accepted 14 August 2023; published 18 September 2023)

High-pressure electrides have opened a promising path to high-temperature superconductors and attracted considerable attention. However, the origins of superconductivity from discrepant sources remain puzzling. In this study, we propose a different type of *p*-orbital-like electride state to shed light on the causality that induces high T_c . Taking our predicted *R*-3m phase in Li_6P as a representative, with a high T_c of 41.36 K, our first-principles studies unveil that the *p*-orbital-like electride states play a dominant role in T_c by softening the acoustic phonon and forming itinerantly hybridized *p*-orbital-like (IHP) electride-states-dependent phonon-coupled bands, which are corroborated by hole doping. Compared to the nonitinerant *s*-orbital-like electride states with low T_c , the IHP electride states exhibit greater freedom of orbital multiplicity and hence a higher propensity to form Cooper pairs, promoting electron-phonon coupling (EPC), and demonstrating the derivation of differential T_c s. Of particular note, the IHP electride states originate from the atypical nature of concurrent oxidation states, characterized by electrons donated from electronegative phosphorus and electropositive lithium. Our finding provides crucial insights into the role of electride states in EPC, elucidates the origin of superconductivity, and identifies the characteristics of high- T_c electrides, with profound implications for exploring this class of multifunctional superconductors.

DOI: [10.1103/PhysRevB.108.L100507](https://doi.org/10.1103/PhysRevB.108.L100507)

The quest for new high-temperature superconductors and elucidating their superconducting mechanisms is a highly compelling subject in condensed matter physics [1–3]. Superconducting electrides, where excess electrons reside at the interstitial regions shaping electride states, have emerged as a new category of conventional BCS-Eliashberg superconductors, inspiring research to develop high-temperature superconducting materials [4–6]. Significant efforts have been devoted to discovering superconducting electrides, including the zero-dimensional (0D) electride $(\text{Ca}_{24}\text{Al}_{28}\text{O}_6)_4^+(e^-)_4$ with an observed T_c of 0.2 K [7], and the Mn_5Si_3 -type Nb_5Ir_3 and Zr_5Sb_3 with T_c s of ~ 2.3 K [8,9]. To search for high- T_c electrides, attention has been focused on electrides under high pressures: the 0D electride Li_6C [10] and the 2D electrides Li_6P [11], Li_5Si [12], and Li_5C [13]. However, the contemporary scales of T_c s proposed above are discrepant and lower than the McMillan limit of 40 K, a benchmark of high- T_c superconductors [14,15]. Consequently, developing multifunctional high- T_c electrides at high pressure has become the frontier task in this field [16]. Indeed, the origins and discrepant effects of superconductivity correlated with

pressure-induced behavior of electride states remain elusive. The electride states in Li_3S [17], Li_5Si , Li_5Sn [12], and Li_6C [10] consistently show a nondominant or even suppressing role in superconductivity, which is in sharp contrast to the electride states of dominant T_c reported in Li_6P [11]. At this stage, it is critical to reveal the mechanisms behind this discrepant behavior of superconductivity and to illustrate the critical factors that either promote or suppress the role of electron-phonon coupling (EPC).

The recently discovered diverse electride states with different T_c s provided crucial clues for investing the superconducting origins. Unlike the isolated electride states, which show insulating characteristics due to the repulsion by core electrons into the lattice interstices [18,19], pressure-induced diversities of dimension and hybridized modes of electride states have led to the emergence of semiconductors, metals, and superconductors [20–24]. Our previous study has shown that 0D *s*-orbital-like electride states exhibiting unexpected ionic and covalent bonds act as a chemical precompression to lower dynamically stable pressure, but are not responsible for EPC, which is consistent with other research results [4,10,17], while 2D electride states are thought to be similar to free electron gases and loosely restricted in the interlayer, which generally show the prospects of conspicuous superconductivity [25,26]. This situation raises fundamental questions about

*Corresponding author: zhuangquan21@outlook.com

†Corresponding author: cuitian@nbu.edu.cn

how the 2D electrider states affect superconductivity and why they are superior to the 0D cases in EPC. With an insufficient superconducting mechanism revealed in previous studies, it is urgently demanded to elucidate the superconducting origination in typical high- T_c 2D electrideres, such as Li_6P , which is of great significance for searching high-temperature superconductivity in multifunctional electrideres.

Our work focuses on revealing the fundamental origin of discrepant superconductivity and identifying the characteristics of high- T_c electrideres. First, we propose an $R-3m$ phase consisting of a different type of p -orbital-like electrideres in Li_6P to address the above-mentioned enigmas. This phase has indistinguishable enthalpies relative to the known $C2/c$ phase above 200 GPa [11], obtained from extensive structure searches in conjunction with first-principles calculations at 0 K. Notably, the T_c of the $R-3m$ phase, which features itinerant p -orbital-like electrider states, is anticipated to be 41.36 K, surpassing the McMillan limit in the BCS-Eliashberg superconductor. In sharp contrast to the low- T_c in s -orbital-like electrideres with nonitinerant electrider states, especially in Li_6C , we found that the remarkable superconductivity of the $R-3m$ phase is primarily due to the strongly phonon-coupled bands and softening of the acoustic phonon related to the hybridized p -orbital-like electrider states. These results directly reveal that the discrepant T_c s in the electrideres are attributed to the electrider states with nonitinerant or itinerant characteristics forming different s - or p -orbital-like and hybridized modes, which have different orbital multiplicity freedoms and influence T_c via Cooper pairs formation. Strikingly, these IHP electrider states are derived from an abnormal nature of concurrent oxidization states; that is, the orbitals of electrider states obtain electrons from both the electronegative element phosphorus and electropositive lithium, revealing a different electrider state formation mechanism. Our study confirms the causal relationship between IHP electrider states and high-temperature superconductivity in electrideres featuring p -orbital-like electrider states. These results would provide a reliable basis for the exploration of high- T_c superconductors in electrideres.

Herein, we undertook multiple routes to predict the high-pressure structures of Li_6P via our in-house developed ELOCR code [27,28] combined with the swarm intelligence-based methodology CALYPSO [29] and evolutionary algorithm USPEX [30]. Our extensive structure search identifies an energetically competitive $R-3m$ phase above 270 GPa, which remains dynamically stable down to 200 GPa [31]. The effect of temperature on phase sequence is displayed in Fig. S1 of the Supplemental Material [31]. As depicted in Fig. 1, this new phase is analogous to the $R-3m$ structure captured in electrideres Li_6Si [41,42] and Li_6C [10], with Li and P atoms occupying the vertices $6h$ ($-0.112\ 28\ -0.112\ 28\ -0.564\ 12$) and center $1b$ ($-0.500\ 00\ -0.500\ 00\ -0.500\ 00$) Wyckoff positions. Given a normal electronegativity relationship, the formal charge of the element phosphorus is supposed to be -3 . We, therefore, infer that the cavity spacing can accommodate up to three extra electrons, resulting in an electrider configuration of $(\text{Li})_6^+(\text{P})_3^{3-}3e^-$, which contains more electrider states than $(\text{Li})_6^+(\text{C})_4^{4-}2e^-$. We then explored the electronic distribution and bonding characteristics using the electron localization function (ELF) [43]. Our analysis revealed that

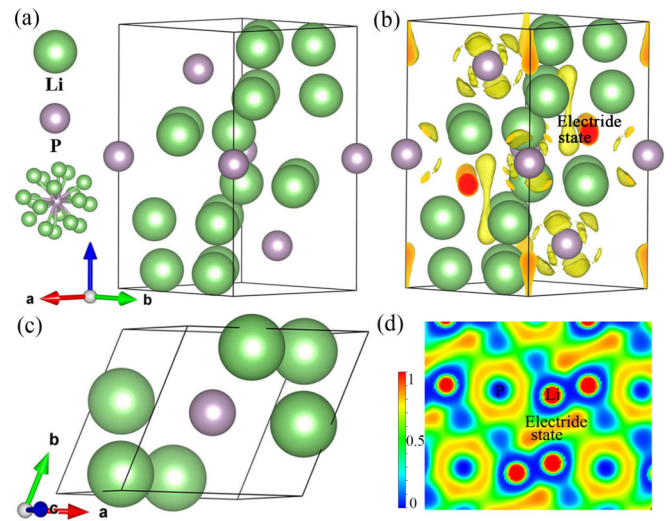


FIG. 1. (a) The $R-3m$ phase at 200 GPa in the hexagonal system and corresponding (b) 3D isosurface plot of electron localization function (ELF) with the partial charge density $0.80e/\text{\AA}^3$, and (c) in the trigonal system and corresponding (d) 2D map of (110) plane.

the excess dumbbell-like electrons shape p -orbital-like electrider states and interconnect each other through intermediate electrons of phosphorus [see Figs. 1(b)–1(d)], which is distinguished from the cagelike electrider states reported in Li_6C [10] and transparent dense sodium [19]. Moreover, the localized Wannier function associated with interstitial electrider state position also demonstrated the p -orbital-like attribute of the electrider states (see Figs. S2 and S3). Further coordination environment analysis demonstrated that this structure comprises 18-coordinated phosphorus atoms within the Li-P bond length of 2.5 Å, indicating strong interactions between Li and P atoms.

To examine whether this electrider with interesting p -orbital-like electrider states provides superconductivity, we have evaluated T_c s for the $R-3m$ phase via the Allen-Dynes-modified McMillan equation [44]. In the pressure range 200–300 GPa, the pressure-dependent superconducting T_c , EPC parameter λ , electronic density of states (DOS) at $\varepsilon_F[N(\varepsilon_F)]$, and logarithmic frequency ω_{\log} of the $R-3m$ phase are summarized in Fig. 2. An estimated T_c of 41.36 K at 200 GPa, surpassing the McMillan limit, is predicted, higher than 39 K of MgB_2 . This indicates that Li_6P with p -orbital-like electrider states has the potential to become a high-temperature superconductor. With increasing pressure up to 290 GPa, T_c decreases monotonically with the coefficient (dT_c/dP) of -0.12 K/GPa. EPC λ decreases for pressures below 270 GPa, increases from 270 to 290 GPa, and trends downward near 300 GPa, while ω_{\log} evolves oppositely. The invariable T_c , in the range 290–300 GPa, is the result of the combined effect of λ and ω_{\log} .

To demystify the origin of relatively high T_c , we need to consider the essential factors for phonon-mediated superconductivity as expounded by BCS theory, including (i) characteristic phonon frequency, (ii) strength of EPC, and (iii) electronic DOS at the ε_F [45]. Given these above-mentioned promising conditions, we then investigate the phonon dispersions, and Eliashberg spectral function $\alpha^2F(\omega)$, along with

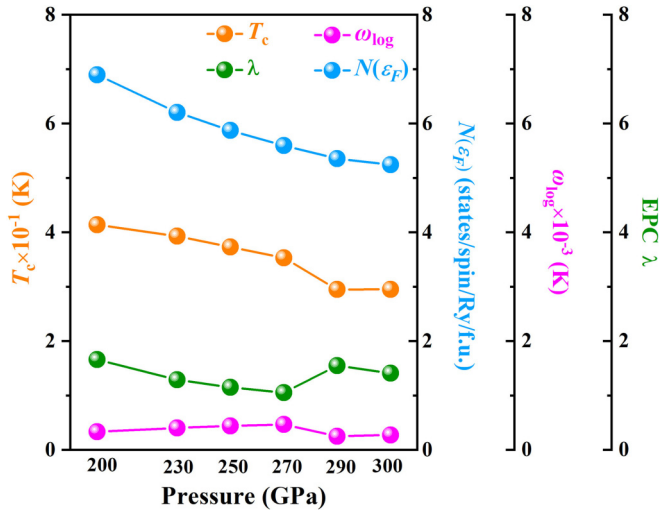


FIG. 2. Calculated superconducting parameters as functions of pressure, including T_c , λ , ω_{\log} , and $N(\varepsilon_F)$ at ε_F .

electron-phonon integral $\lambda(\omega)$ and $N(\varepsilon_F)$ for the $R-3m$ phase of Li_6P at 200 GPa.

On the aspect of phonon DOS, as shown in Fig. 3(a), the lithium-associated phonons below 8 THz strongly couple with electrons, contributing 75% to total EPC. Remarkably, the soft phonon mode below 5 THz has a significant impact on enhancing the EPC, which is reflected by the large pro-

jected phonon linewidths, integral EPC strength $\lambda(\omega)$, and a high peak in the Eliashberg $\alpha^2F(\omega)$. The optical phonons with larger frequencies afford a broader range of energy from various vibrational modes, enhancing the likelihood of satisfying the formation energy of Cooper pairs, which is beneficial for achieving high T_c . This can be proved by the strong dependency of optical phonon frequencies on wave vector, and this feature, electrons being intensively scattered by optical phonons, is also observed in H_3S [46]. Especially from 5 to 15 THz, the high broadening of phonon vibrations coupled with high-weighted projected phonon linewidths suggests that dumbbell-like electrider states may collaborate with Li and P atoms to form a strong interatomic coupling effect, which also leads to the adjacent atoms being tightly bound to form a denser structure and scattering electrons to promote EPC.

To elucidate the deep-seated causation of phonon softening below 5 THz, the Fermi surface (FS) nesting based on the nesting function, $\xi_{\mathbf{q}} = \frac{1}{N} \sum_{\mathbf{k}, i, j} \delta(\varepsilon_{\mathbf{k}, i} - \varepsilon_F) \times \delta(\varepsilon_{\mathbf{k}+\mathbf{q}, j} - \varepsilon_F)$, has been plotted in Fig. 3(b). The routes of phonon softening corresponding to the correlative nesting vectors span Q points along $Q_{\Gamma} \rightarrow Q_F$. Meanwhile, a strongly nested point corresponding to the softening phonon mode in the medial interval between Q_{Γ} and Q_Z is also conspicuous. These strongly indicate that the soft phonon modes derive from the FS nesting [47,48]. Likewise, the occurrence of FS nesting is anticipated, and the quantitative results of $\xi_{\mathbf{q}}$ can be proved by the FS and electronic band conformation in

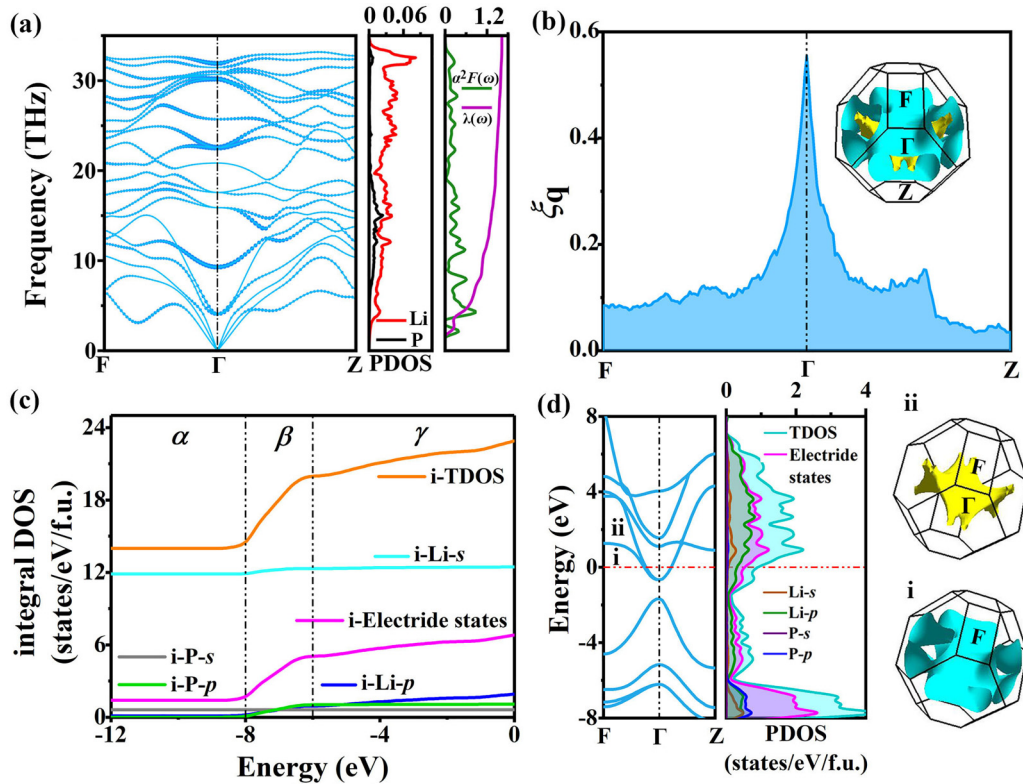


FIG. 3. (a) Phonon dispersion, projected phonon DOS, and $\alpha^2F(\omega)$ with electron-phonon integral $\lambda(\omega)$ at 200 GPa. The solid blue dot on the phonon spectra represents the contribution of the phonon linewidth in proportion to the spherical scale. (b) Nesting function $\xi_{\mathbf{q}}$ along typical \mathbf{q} paths and the illustration of FS. (c) Integral DOS values of different atoms up to ε_F on a per f.u. basis. (d) Band structures and projected DOS (PDOS) of $R-3m$ phase at 200 GPa.

Figs. 3(b) and 3(d), where two conduction bands cross the ε_F , and the electron velocities on the opposite faces of the “sake cup” and “catheter” shaped portions are parallel to each other. Moreover, the degrees of phonon softening vary for different phonon modes at the same \mathbf{q} vector, which may be related to the electron-phonon matrix element $g_{mn}^{\nu}(\mathbf{k}, \mathbf{q})$ mirrored by phonon linewidth $\gamma_{\mathbf{q}\nu}$, as reflected by the thickness of the linewidth in the phonon band [see Fig. 3(a)]. That is because the phonon linewidth $\gamma_{\mathbf{q}\nu}$ is mainly affected by two factors: the nesting function $\xi_{\mathbf{q}}$ and the electron-phonon matrix element $g_{mn}^{\nu}(\mathbf{k}, \mathbf{q})$ based on the formula $\gamma_{\mathbf{q}\nu} = \pi \omega_{\mathbf{q}\nu} \sum_{mn} \sum_{\mathbf{k}} |g_{mn}^{\nu}(\mathbf{k}, \mathbf{q})|^2 \delta(\varepsilon_{\mathbf{k},i} - \varepsilon_F) \times \delta(\varepsilon_{\mathbf{k}+\mathbf{q},j} - \varepsilon_F)$.

On the aspect of electronic DOS, we investigated the contributions related to the dumbbell-like electrider states and the potential hybridization, as presented in Figs. 3(c) and 3(d). The band structure reveals metallic properties characterized by the abundant occupation of double p -orbital hybridized electronic states at ε_F . These states involve electrider states p and Li- p orbitals and that form strongly phonon-coupled bands owing to bands hopping being ~ 5 eV. The electrider states have typical p -electronic characteristics as proved by PDOS. Our further analysis uncovered that the hybridized p -orbital-like electrider states originate from an unusual formation process of oxidization states. This was confirmed by the transfer of valence electrons from the P- s/p and Li- s to electrider-states- p orbitals, forming the $(\text{P})^{\sigma+}$ oxidization states of phosphorus. To demonstrate the formation mechanism of this type of p -orbital-like electrider states and double p -orbital hybridizations, we divided the integral DOS into three blocks, marked as α , β , and γ , as depicted in Fig. 3(c). Block α is a characteristic of the forbidden zone of charges. Being attributed to abundant electrons deficiency from P- p and Li- s orbitals that assemble to electrider-states- p and Li- p orbitals, block β is an intense zone of unusual charge transfer, forming characteristics of double p -orbital-like hybridizations. Block γ is a relatively weak zone of charge transfer because only a small part of electrons derived from P- s/p and Li- s orbitals are transferred to electrider-states- p and Li- p orbitals. This pressure effect induces an unusual nature of concurrent oxidization states, demonstrating a nonclassical formation mechanism of electrider states with a configuration of $(\text{Li})_6^{\delta+}(\text{P})^{\sigma+}6.86e^-$ ($6 \times \delta + \sigma = 6.86$).

In stark contrast to the mechanism of superconductivity induced by pressure, which involves a transition from s states to non- s states forming sp hybridizations in alkali metals, the superconducting Li_6P mainly stems from the hybridized effect between electrider-states- p and Li- p electrons. These hybridized p -orbital electronic states have a strong coupling with the fundamental vibrations of constituent Li atoms, as evidenced by the electronic band structure in Fig. 3(d). In this figure, two highly dispersed paraboliclike bands with high group velocities (see Fig. S4 [31]) cross ε_F . The band-structure analysis, in turn, corroborates the bonding picture observed in real space: electrider states stabilized by the $(\text{Li})_6^{\delta+}$ and $(\text{P})^{\sigma+}$ cations, with which electrider states form strong ionic bonds as shown in Fig. 1(d) [49]. Furthermore, electrider states retain a free-electron-like behavior to participate in EPC, which can be verified by the following two aspects. (i) The number of integral electrider states intensively aggregates with pressurization, from 200 to 300 GPa, and steadily ac-

counts for almost $\sim 26\%$ (see Fig. S5 [31]). (ii) As the lattice cavity is suppressed with pressurization by the coefficient (dV/dP) of $-0.0458 \text{ \AA}^3/\text{GPa}$, the reduction ratio of electrider states, $-0.008 \text{ states/f.u./GPa}$, is negligible (see Fig. S6 [31]), indicating a nearly constant total amount of electrider states with the reduction of the lattice volume ($d \text{ states}/dV$, 0.0017) and the itinerant of electrider states.

Being directly proportional to the evolution of T_c with pressurization (see Fig. 2), the electronic DOS at ε_F is thus disclosed to dominate the variation trend of T_c s, in which the prominent role of hybridized double p -orbital electronic states determining the superconducting T_c is consequently identified. This role is further verified by analyzing the effect of hole doping, which neutralizes the p -orbital-like electrons. As demonstrated in Fig. 4(a), the integral DOS values for electrider-state- p and Li- p at the doping level of $n_h = 1e$ are significantly lower than in the undoped case. Regarding the distinctly regulating effect on superconductivity, the hole-doping-dependent superconducting parameters and $N(\varepsilon_F)$ at 200 GPa are calculated and depicted in Fig. 4(b). T_c gradually decreases with the increasing doping concentration and vanishes at a level higher than $1e$.

To further elaborate on the role of the IHP electrider states on superconductivity, the electronic structures, phonon spectrum, and EPC at $n_h = 1e$ are studied and compared with the undoped case at 200 GPa. In addition to forming a pseudoenergy gap [50] derived from the shifting down of ε_F induced by hole doping [Fig. 4(e)], a significant disappearance of softened acoustic phonons is also observed [Fig. 4(c)]. Consequently, the value of EPC λ shows a remarkable reduction of 87.5% compared with the case of undoped Li_6P . From the frequency dependence of $\lambda(\omega)$, we found that about two-thirds of the reduced total EPC λ results from acoustic phonons, which are the primary component of EPC for scattering electrons. The hole-doping-induced soft-mode vanishing derives from the disappearance of FS nesting, as indicated by the nesting functions $\xi_{\mathbf{q}}$ in Fig. 4(d). The FS nesting was proven to be dominated by the electrider states in hybridized p electrons, according to the proportional relationship between Li- p and electrider-state- p -like orbitals at different doping levels delineated in Fig. 4(f). This directly demonstrates the prominent role of electrider states in FS nesting, thus the phonon softening and EPC. Moreover, on account of the sharply declined peak above 5 THz of $\alpha^2F(\omega)$ at $n_h = 1e$, the contribution of this part of phonons to EPC was significantly reduced. Based on the hole-doping analysis described above, we concluded that the disappearance of T_c induced by IHP electrider states could be mainly attributed to three factors: (i) the absence of soft-mode effects in acoustic branches, (ii) the weakened interatomic bonding interaction derived from participation of electrider states, and (iii) the descent of itinerant electrons constituting Cooper pairs at the FS.

By further comparison with the insulating characteristic of $(\text{Li}^+)_3\text{P}^{3-}$, the IHP electrider states in Li_6P , with the configuration of $(\text{Li})_6^{\delta+}(\text{P})^{\sigma+}6.86e^-$, are demonstrated to enhance the coupling effects between Li and P atoms, participating in EPC and enhancing superconductivity. Meanwhile, in sharp contrast to the low T_c of s -orbital-like electrider Li_6C [10], Li_5Si , and Li_5Sn [12] induced by nonitinerantly electrider states, recently reported examples suggest that hybridized p -orbital-

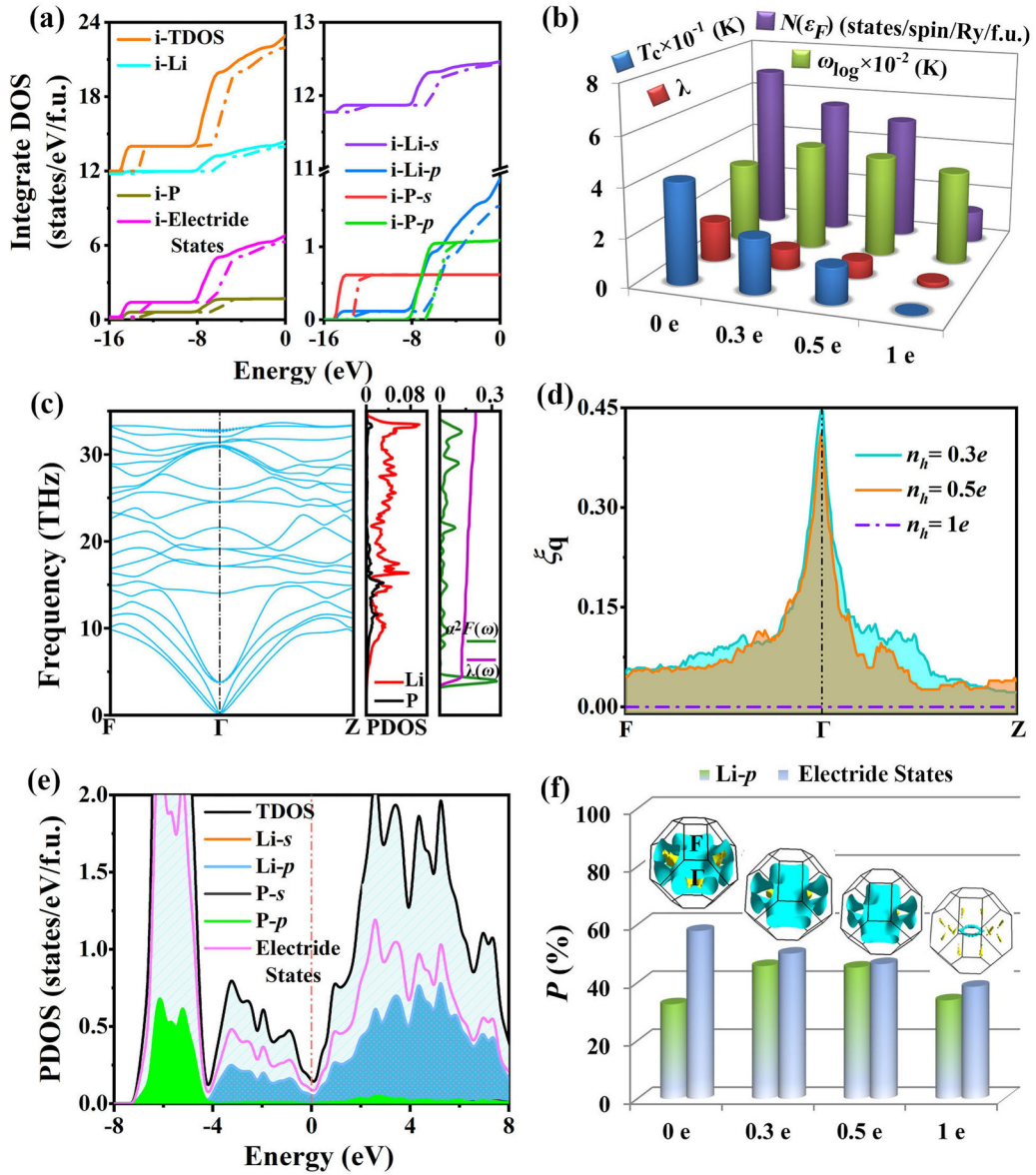


FIG. 4. The hole-doping modulated electronic properties and superconductivity at 200 GPa. (a) Integral DOS values of different elements up to ϵ_F (set to zero) without hole doping (the solid line) and at doping level (n_h) of $1e$ (dashed line). (b) The calculated T_c , $\lambda(\omega)$, ω_{\log} , and $N(\epsilon_F)$ with different hole doping concentrations. (c) Phonon dispersion, projected phonon DOS, and $\alpha^2 F(\omega)$ along with integral $\lambda(\omega)$ at $n_h = 1e$. (d) The nesting function ξ_q with different doping concentrations. (e) PDOS at $n_h = 1e$. (f) Contribution percentages of electride-states- p and Li- p to $N(\epsilon_F)$ and the corresponding 3D FS at different doping levels.

like electrides possess high T_c . This potential is attributed to the IHP electride states' freedoms of orbital multiplicity being higher than s block, giving them a stronger ability to form Cooper pairs and to promote EPC [51,52]. Instructively, our discovery of $R-3m-CdCl_2$ -type Li_6P with IHP electride states and notable T_c highlights the correlation between new IHP electride states and novel superconductors.

To test the above-mentioned correlation and identify more characteristics of high- T_c electrides induced by IHP electride states, we searched for new p -orbital-like electrides from the CALYPSO database by screening p -block elements that easily form concurrent oxidation states. Here, the $C2/m-Li_9Te$ and $C2/m-Li_{10}Se$ are verified to be dumbbell-like p -orbital-like electrides (see Figs. S9 and S10 [31]) with

predicted T_c s of 10.2 K at 75 GPa [24] and 16 K at 50 GPa [53], respectively. The T_c s higher than in typical s -orbital-like electrides [10,52] mainly originated from the coupling between hybridized p -orbital-like electride states and the non- s -states of other elements. Intriguingly, our in-depth analysis reveals that these p -orbital-like characteristics are induced through synergistic oxidation states, which is also reflected in the $C2/c-Li_6P$ as shown in Fig. S11. Consistent with our view of searching the p -orbital-like electride states, nother research [53] shows that the selection of p -orbital-like elements is beneficial for producing high- T_c electrides while the internal causality referring to electride states was not revealed. Our research confirms the close relationship between our proposed p -orbital-like electride states and

superconductivity, providing a reliable basis for searching multifunctional high- T_c superconductors.

In conclusion, we report a type of p -orbital-like electrider state that dominates high-temperature superconductivity in electrides. Our predicted electrider $R-3m\text{-Li}_6\text{P}$ was selected as a representative to understand the role of p -orbital-like electrider states on EPC and to elucidate the origin of superconductivity, which is subjected to multiple structure searches combined with extensive first-principles calculations for the analysis of its electronic structures, bonding properties, and superconducting origin. In sharp contrast to the nonitinerantly electrider states in s -orbital-like electrides with low- T_c , our predicted electrider exhibits exceptional superconductivity with a T_c of 41.36 K surpassing the McMillan limit, mainly attributed to the strong EPC derived from the lattice contributions and phonon softening bands dominated by IHP electrider states with higher freedoms of orbital multiplicity. The formation of p -orbital-like electrider states originates from an unusual concurrent oxidization state of elements lithium and phosphorus. Our study not only reveals the promoting effect

of hybridized p -orbital-like electrider states on EPC, but also crucially identifies the characteristics of high- T_c electrides, which have extensive implications for comprehending the origins of superconductivity and exploring high- T_c superconductors in electrides.

We thank Prof. Y. Zhang for helpful discussions on the Wannier functions. This work was supported by the National Natural Science Foundation of China (Grants No. 52072188, No. 12264038, No. 12304021, and No. 11904187), Zhejiang Provincial Natural Science Foundation of China (Grant No. LQ23A040004), Program for Science and Technology Innovation Team in Zhejiang (Grant No. 2021R01004), Program for Changjiang Scholars and Innovative Research Team in University (Grant No. IRT_15R23), and Natural Science Foundation of Inner Mongolia (Grant No. 2022MS01013). Parts of calculations were performed at the Supercomputer Center of NBU.

The authors declare no conflict of interest.

-
- [1] A. P. Drozdov, P. P. Kong, V. S. Minkov, S. P. Besedin, M. A. Kuzovnikov, S. Mozaffari, L. Balicas, F. F. Balakirev, D. E. Graf, V. B. Prakapenka *et al.*, *Nature (London)* **569**, 528 (2019).
- [2] M. Somayazulu, M. Ahart, A. K. Mishra, Z. M. Geballe, M. Baldini, Y. Meng, V. V. Struzhkin, and R. J. Hemley, *Phys. Rev. Lett.* **122**, 027001 (2019).
- [3] K. Hilleke and E. Zurek, *Angew. Chem. Int. Ed.* **134**, e202207589 (2022).
- [4] M. S. Miao and R. Hoffmann, *Acc. Chem. Res.* **47**, 1311 (2014).
- [5] M. S. Miao and R. Hoffmann, *J. Am. Chem. Soc.* **137**, 3631 (2015).
- [6] P. V. Sushko, A. L. Shluger, K. Hayashi, M. Hirano, and H. Hosono, *Phys. Rev. Lett.* **91**, 126401 (2003).
- [7] S. Tanaka, T. Kato, A. Miyake, T. Kagayama, K. Shimizu, S. W. Kim, S. Matsuishi, and H. Hosono, *J. Korean Phys. Soc.* **63**, 477 (2013).
- [8] Y. Zhang, B. Wang, Z. Xiao, Y. Lu, T. Kamiya, Y. Uwatoko, H. Kageyama, and H. Hosono, *npj Quantum Mater.* **2**, 45 (2017).
- [9] B. Lv, X. Y. Zhu, B. Lorenz, F. Y. Wei, Y. Y. Xue, Z. P. Yin, G. Kotliar, and C. W. Chu, *Phys. Rev. B* **88**, 134520 (2013).
- [10] Z. Liu, Q. Zhuang, F. Tian, D. Duan, H. Song, Z. Zhang, F. Li, H. Li, D. Li, and T. Cui, *Phys. Rev. Lett.* **127**, 157002 (2021).
- [11] Z. Zhao, S. Zhang, T. Yu, H. Xu, A. Bergara, and G. Yang, *Phys. Rev. Lett.* **122**, 097002 (2019).
- [12] J. Y. You, B. Gu, G. Su, and Y. P. Feng, *J. Am. Chem. Soc.* **144**, 5527 (2022).
- [13] Z. S. Pereira, G. M. Faccin, and E. Z. da Silva, *J. Phys. Chem. C* **125**, 8899 (2021).
- [14] X. H. Chen, T. Wu, G. Wu, R. H. Liu, H. Chen, and D. F. Fang, *Nature (London)* **453**, 761 (2008).
- [15] W. L. McMillan, *Phys. Rev.* **167**, 331 (1968).
- [16] L. Zhang, Y. Wang, J. Lv, and Y. Ma, *Nat. Rev. Mater.* **2**, 17005 (2017).
- [17] C. Kokail, C. Heil, and L. Boeri, *Phys. Rev. B* **94**, 060502(R) (2016).
- [18] M. S. Miao, R. Hoffmann, J. Botana, Naumov, II, and R. J. Hemley, *Angew. Chem. Int. Ed.* **56**, 972 (2017).
- [19] Y. Ma, M. Eremets, A. R. Oganov, Y. Xie, I. Trojan, S. Medvedev, A. O. Lyakhov, M. Valle, and V. Prakapenka, *Nature (London)* **458**, 182 (2009).
- [20] H. Tang, B. Wan, B. Gao, Y. Muraba, Q. Qin, B. Yan, P. Chen, Q. Hu, D. Zhang, L. Wu *et al.*, *Adv. Sci.* **5**, 1800666 (2018).
- [21] M. Miao, Y. Sun, E. Zurek, and H. Lin, *Nat. Rev. Chem.* **4**, 508 (2020).
- [22] Y. Zhang, W. Wu, Y. Wang, S. A. Yang, and Y. Ma, *J. Am. Chem. Soc.* **139**, 13798 (2017).
- [23] S. Y. Lee, J. Hwang, J. Park, C. N. Nandadasa, Y. Kim, J. Bang, K. Lee, K. H. Lee, Y. Zhang, Y. Ma *et al.*, *Nat. Commun.* **11**, 1526 (2020).
- [24] X. Zhang, F. Li, A. Bergara, and G. Yang, *Phys. Rev. B* **104**, 134505 (2021).
- [25] W. Ming, M. Yoon, M. H. Du, K. Lee, and S. W. Kim, *J. Am. Chem. Soc.* **138**, 15336 (2016).
- [26] Y. Tsuji, P. Dasari, S. F. Elatresh, R. Hoffmann, and N. W. Ashcroft, *J. Am. Chem. Soc.* **138**, 14108 (2016).
- [27] Q. Zhuang, X. Jin, Q. Lv, Y. Li, Z. Shao, Z. Liu, X. Li, H. Zhang, X. Meng, K. Bao *et al.*, *Phys. Chem. Chem. Phys.* **19**, 26280 (2017).
- [28] S. Yang, Q. Zhuang, X. Jin, L. Song, L. Zhang, T. Cui, and B. Liu, *Phys. Rev. B* **103**, 174520 (2021).
- [29] Y. Wang, J. Lv, L. Zhu, and Y. Ma, *Phys. Rev. B* **82**, 094116 (2010).
- [30] A. R. Oganov and C. W. Glass, *J. Chem. Phys.* **124**, 244704 (2006).
- [31] See Supplemental Material at <http://link.aps.org/supplemental/10.1103/PhysRevB.108.L100507> for detailed superconducting calculations, structural information, calculated enthalpies for

- Li₆P structures, calculated Wannier function, integral DOS values, phonon dispersion, $\alpha^2 F(\omega)$ and integral $\lambda(\omega)$ of hole-doping; projected density of states, FS of the $R-3m$ phase with a projection of the Fermi velocity, 3D FS at different doping levels, and electronic structural properties of Li₉Te, Li₁₀Se, and Li₆P. It also contains Refs. [32–40].
- [32] G. Kresse and J. Furthmüller, *Phys. Rev. B* **54**, 11169 (1996).
- [33] P. E. Blochl, *Phys. Rev. B* **50**, 17953 (1994).
- [34] P. Giannozzi, S. Baroni, N. Bonini, M. Calandra, R. Car, C. Cavazzoni, D. Ceresoli, G. L. Chiarotti, M. Cococcioni, I. Dabo *et al.*, *J. Phys.: Condens. Matter* **21**, 395502 (2009).
- [35] A. A. Mostofi, J. R. Yates, Y. S. Lee, I. Souza, D. Vanderbilt, and N. Marzari, *Comput. Phys. Commun.* **178**, 685 (2008).
- [36] Y. Wu, P. Lazic, G. Hautier, K. Persson, and G. Ceder, *Energ. Environ. Sci.* **6**, 157 (2013).
- [37] F. Peng, Y. Sun, C. J. Pickard, R. J. Needs, Q. Wu, and Y. Ma, *Phys. Rev. Lett.* **119**, 107001 (2017).
- [38] H. Bi, S. Zhang, S. Wei, J. Wang, D. Zhou, Q. Li, and Y. Ma, *Phys. Chem. Chem. Phys.* **18**, 4437 (2016).
- [39] H. Liu, I. I. Naumov, Z. M. Geballe, M. Somayazulu, J. S. Tse, and R. J. Hemley, *Phys. Rev. B* **98**, 100102(R) (2018).
- [40] I. Errea, M. Calandra, C. J. Pickard, J. Nelson, R. J. Needs, Y. Li, H. Liu, Y. Zhang, Y. Ma, and F. Mauri, *Phys. Rev. Lett.* **114**, 157004 (2015).
- [41] W. W. Tipton, C. R. Bealing, K. Mathew, and R. G. Hennig, *Phys. Rev. B* **87**, 184114 (2013).
- [42] I. Valencia-Jaime, R. Sarmiento-Pérez, S. Botti, M. A. L. Marques, M. Amsler, S. Goedecker, and A. H. Romero, *J. Alloys Compd.* **655**, 147 (2016).
- [43] A. D. Becke and K. E. Edgecombe, *J. Chem. Phys.* **92**, 5397 (1990).
- [44] P. B. Allen and R. C. Dynes, *Phys. Rev. B* **12**, 905 (1975).
- [45] H. Xie, Y. Yao, X. Feng, D. Duan, H. Song, Z. Zhang, S. Jiang, S. A. T. Redfern, V. Z. Kresin, C. J. Pickard *et al.*, *Phys. Rev. Lett.* **125**, 217001 (2020).
- [46] Q. Zhuang, X. Jin, T. Cui, D. Zhang, Y. Li, X. Li, K. Bao, and B. Liu, *Phys. Rev. B* **98**, 024514 (2018).
- [47] Y. Ma, D. Duan, Z. Shao, H. Yu, H. Liu, F. Tian, X. Huang, D. Li, B. Liu, and T. Cui, *Phys. Rev. B* **96**, 144518 (2017).
- [48] J. S. Tse, Y. Yao, and K. Tanaka, *Phys. Rev. Lett.* **98**, 117004 (2007).
- [49] M. Gao, X.-W. Yan, Z.-Y. Lu, and T. Xiang, *Phys. Rev. B* **104**, L100504 (2021).
- [50] P. Vajeeston, P. Ravindran, C. Ravi, and R. Asokamani, *Phys. Rev. B* **63**, 045115 (2001).
- [51] C. Wang, S. Yi, and J.-H. Cho, *Phys. Rev. B* **101**, 104506 (2020).
- [52] H. Hosono, S. W. Kim, S. Matsuishi, S. Tanaka, A. Miyake, T. Kagayama, and K. Shimizu, *Philos. Trans. R. Soc., A* **373**, 20140450 (2015).
- [53] X. Zhang, Y. Zhao, A. Bergara, and G. Yang, *J. Chem. Phys.* **156**, 194112 (2022).